Smart Structures and Systems, *Vol. 31*, *No. 5* (*2023*) *485-500*
https://doi.org/10.12989/sss.2023.31.5.485

Hybrid machine learning with mode shape assessment for damage identification of plates

Pei Yi Siow [1], Zhi Chao Ong[*1,2], Shin Yee Khoo [1,2], Kok-Sing Lim [3] and Bee Teng Chew [1]

[1] *Department of Mechanical Engineering*, *Faculty of Engineering*, *Universiti Malaya*, *50603 Kuala Lumpur*, *Malaysia*
[2] *Centre of Research Industry 4.0* (*CRI 4.0*), *Faculty of Engineering*, *Universiti Malaya*, *50603 Kuala Lumpur*, *Malaysia*
[3] *Photonics Research Centre*, *Deputy Vice Chancellor* (*Research & Innovation*) *Office*, *Universiti Malaya*, *50603 Kuala Lumpur*, *Malaysia*

(*Received June 6*, *2022*, *Revised November 26*, *2022*, *Accepted March 17*, *2023*)

Abstract. Machine learning-based structural health monitoring (ML-based SHM) methods are researched extensively in the recent decade due to the availability of advanced information and sensing technology. ML methods are well-known for their pattern recognition capability for complex problems. However, the main obstacle of ML-based SHM is that it often requires pre-collected historical data for model training. In most actual scenarios, damage presence can be detected using the unsupervised learning method through anomaly detection, but to further identify the damage types would require prior knowledge or historical events as references. This creates the cold-start problem, especially for new and unobserved structures. Modal-based methods identify damages based on the changes in the structural global properties but often require dense measurements for accurate results. Therefore, a two-stage hybrid modal-machine learning damage detection scheme is proposed. The first stage detects damage presence using Principal Component Analysis-Frequency Response Function (PCA-FRF) in an unsupervised manner, whereas the second stage further identifies the damage. To solve the cold-start problem, mode shape assessment using the first mode is initiated when no trained model is available yet in the second stage. The damage identified by the modal-based method would be stored for future training. This work highlights the performance of the scheme in alleviating the cold-start issue as it transitions through different phases, starting from zero damage sample available. Results showed that single and multiple damages can be identified at an acceptable accuracy level even when training samples are limited.

Keywords: frequency response function; machine learning; mode shape; principal component analysis; structural damage identification

1. Introduction

Modal-based damage identification methods have gained much attention among researchers due to the direct relationship between structural damages and the changes in the modal parameters, i.e., natural frequencies and mode shapes. Any changes in the modal parameters, which describe the structural dynamic behavior, indicate possible damages due to the changes in the stiffness of the structure. Using the changes in natural frequency to detect damage (Mekjavic and Damjanovic 2017, Sha *et al*. 2019) is the most straightforward modal-based approach, but it could be insensitive to light damage on large and complex structures. Mode shapes are rich in spatial properties and have shown to be effective in identifying damages from simpler structures such as plates (Abdulkareem *et al*. 2019) and beams (Xu *et al*. 2020), to complex structures such as railway sleepers (Janeliukstis *et al*. 2019) and suspension bridges (Wickramasinghe *et al*. 2020). The main factors that affect the accuracy of mode shape-based methods are noise and spatial completeness (Wang and Xu 2019). However, natural frequencies and mode shapes are not the upstream data as they need to be extracted from the Frequency response functions (FRFs) through modal parameter extraction process. Thus, the modal parameters could incur errors from the modal parameter extraction process, which can further affect their damage sensitivity. As the FRFs itself is already rich and compact with dynamic information, using them as the damage sensitive features could eliminate the errors due to modal parameter extraction. Works from Xu *et al*. (2014) and Porcu *et al*. (2019) proved that the FRF-based and the FRF curvature methods are more damage sensitive than natural frequency-based and mode shape-based methods. The main challenge for the FRF-based method is the high dimensionality of data, especially when dense measurements are included. Therefore, dimension reduction algorithms such as Principal Component Analysis (PCA) are commonly applied to extract the main features of the FRFs, so that lower-dimension FRFs can be constructed and used for damage identification (Li *et al*. 2011, Padil *et al*. 2020). Generally, several works have shown the effectiveness of PCA in compressing the FRFs by filtering noises and improving their sensitivity to light damage (Bandara *et al*. 2014, Jayasundara *et al*. 2020) and measurement errors (Esfandiari *et al*. 2020, Siow *et al*. 2021). Clean modal data is important for accurate damage identification when any modal-based method is used. Apart from using PCA for

*Corresponding author, Ph.D., Associate Professor,
E-mail: zhichao83@gmail.com; alexongzc@um.edu.my

ISSN: 1738-1584 (Print), 1738-1991 (Online)

noise removal at the frequency domain, another method is by removing the noises at the time domain such as applying Impact-Synchronous Modal Analysis (ISMA), which is an alternative modal analysis technique. ISMA is an input-output method that allows the test structure to be in either static or operating conditions, where operating noises can be suppressed by using the Impact-Synchronous Time Averaging technique (Lim *et al*. 2019, Ong *et al*. 2019). This approach produces clean static-like FRFs which can be directly used for damage identification. Recent work has shown its applicability in damage identification (Chen *et al*. 2020a), where clean FRFs can be obtained for modal parameter extraction. Overall, modal data quality is the main factor of accurate damage identification when using modal-based methods.

With the increasing availability of advanced sensing equipment and cloud devices, machine learning-based methods, also known as data-driven methods, are more widely used in structural health monitoring nowadays. Machine learning algorithms can process a large amount of complex data with minimum human intervention. The two main categories of machine learning algorithms are supervised and unsupervised learning algorithms. Supervised models such as Artificial Neural Networks (ANN) and Convolutional Neural Networks (CNN) are trained with labelled data, where they learn the relationship between the input features and the labels. The recent decade has shown that supervised models are highly accurate in damage identification (Jayasundara *et al*. 2020, Nguyen *et al*. 2020, Nick *et al*. 2021) when they have sufficient training data and classes. However, it is expensive and not practical to collect real damage data before developing the damage detection model in most actual scenarios, which often leads to incomplete training data that can reduce the accuracy in identifying new types of damage. Insufficient training data leads to the cold-start problem, which is commonly faced by new and unobserved structures. Therefore, unsupervised damage detection models are more commonly used in practice as they do not require labelled data and training. Unsupervised algorithms such as k-means and hierarchical cluster the samples into several groups based on the data feature, thus helping experts to visualize the overall data partition before interpreting them. The anomaly detection approach is commonly used as the unsupervised damage detection method, where the undamaged data is treated as the baseline data and outliers as the damaged data (Chen *et al*. 2022, Solimine *et al*. 2020). For most unsupervised-based damage detection methods, vibration-based features, condition parameters and statistical scores from raw data are used as the input features (Sarmadi *et al*. 2021). These features are then correlated together with structural damage and then manually labelled by experts. However, the relationship built may not globally represent the model, which can affect the damage sensitivity of the features and the damage identification accuracy of the model due to uncertainties.

Therefore, modal-based machine learning damage identification methods are investigated, where modal parameters are used as the machine learning input features. As the change in the modal parameters is directly related to structural damages, they can be used as the input features of a machine learning-based damage scheme. Some works have shown that the modal-based machine learning schemes, particularly supervised methods, have good damage identification accuracy even with few measurement points, which proves the global representation of modal parameters in structural damage (Cevasco *et al*. 2022, Chang *et al*. 2018, Ghannadi and Kourehli 2019, Vafaei and Alih 2018). It is also highlighted in these works that modal data quality is an important factor for accurate damage identification results. As for a modal-based unsupervised approach, Chen *et al*. applied hierarchical clustering with waveform chain code analysis for damage identification, and PCA-reduced FRFs are used as the damage sensitive features. Results showed that the proposed method can detect damage presence and further cluster the dataset into different damage locations and severities (Chen *et al*. 2020b).

Generally, the only difference between modal-based machine learning damage identification methods and other machine learning damage identification methods is the types of features used, where the overall working principle is still the same. Therefore, cold-start and manual labelling issues still exist. In short, the choice of machine learning method depends on the availability of labelled damage samples, i.e., either a supervised model if there are sufficient labelled samples which is usually rare, or an unsupervised model if there are no or limited labelled samples. New or unobserved structures would have no choice but to implement the unsupervised method as there are none or limited labelled damage samples available. As unsupervised methods do not assign labels to the samples, human interpretation and manual labelling efforts are required after clustering, which makes them only practical for detecting damage presence. A supervised method can be added after unsupervised damage presence detection to auto-label the clusters, but it is only applicable when it has been trained with sufficient damage events. Manual labelling becomes an issue, especially when a large dataset is involved. Labels are needed for the clusters generated from unsupervised models and samples for supervised model training. Recent works have shown the potential of semi-supervised or active learning in auto-labelling using a few labelled samples (Bull *et al*. 2018, 2019). However, the few labelled samples will still require manual labelling effort, thus, not being fully automated. More labelled samples may also be required in actual scenarios for better accuracy, thus requiring much more manual labelling efforts. Therefore, a physics-based method such as a modal-based method, which uses physically interpretable features that have a global representation of the structure, could be strategically integrated with machine learning methods to combat the cold-start and manual labelling issues. Although solely using a modal-based method could be sufficient since it has a good representation of the model, detailed experiments and computational analysis may be required beforehand to investigate the generalization of the method. As supervised models such as ANN are trained through building relationship between the input features and the output, using a supervised model when there are sufficient

labelled samples can help to generalize the modal-based damage scheme. Therefore, this work proposes a two-stage hybrid modal-machine learning damage assessment scheme. The first stage employs the unsupervised method to detect damage presence. Instead of modal parameters, the PCA-FRF, the upstream data, is used as the damage sensitive feature in the first stage to minimize estimation errors from modal parameter extraction. The unsupervised method is also placed at the first stage to overcome the cold-start issue faced by supervised method, thus applicable to new or unobserved structures. The second stage, i.e., the damage identification stage, would only be initiated when damage presence is detected at the first stage. To overcome the cold-start and manual labelling issues faced by supervised methods in damage identification, a modal-based method, i.e., mode shape assessment, is placed at the second stage. The first mode shape difference, which is found to be directly related to damages, is used to identify and auto-label the damage. The labelled damage samples will then be stored in a database for future supervised training purposes. When there are sufficient labelled damage samples, supervised training is initiated to aid in generalizing the scheme in predicting multiple damages. Overall, the main contribution of this work is an integration strategy of a mode shape-based method and machine learning methods to combat the manual labelling and cold-start issues faced by machine learning-based damage assessment schemes. The novelty of the proposed method is the implementation strategy of the mode shape assessment-based method to bridge the unsupervised and supervised methods, solving the cold-start and manual labelling issues. The authors would also wish to highlight that this study is a continuation of a previously published investigation (Siow *et al*. 2021), which has proven the damage sensitivity of PCA-FRF in detecting damage presence in an unsupervised manner.

2. Theoretical background

2.1 PCA-FRF damage sensitive feature

High dimensional data not only requires more computational power to be processed by machine learning models but could also have lower data sensitivity as it could contain noises and insignificant features. The FRFs can be very complex when dense measurement points and wide frequency range are used. PCA, which is a dimension reduction algorithm, is commonly used to compress the FRFs before being analysed by machine learning models. In general, the PC indicates the position of the original data in the corresponding principal components. The first principal component (PC1) would indicate the direction of the original data consisting of the maximum variance (eigenvalue). The next principal component, i.e., PC2 would be orthogonal to PC1 with maximum variance, and so on. As the number of principal component increases, the variance decreases, meaning the contribution of the main features from the original data decrease.

For this study, the first two principal components, i.e., PC1 and PC2 were selected to build the single-lined PCA-FRF because they have a cumulative contribution (cumulative variance) of more than 99.9%, which means that the first two PCs are sufficient to represent the original 5-lines-FRFs by 99.9% based on the published study (Siow *et al*. 2021). It was also proven that when PCA is applied, not only the dimensions of the FRFs can be reduced, but the resonance peaks can be retained, and the damage sensitivity can be improved, where the shift of the damaged data from the undamaged data is exaggerated. PC1 was used as the x-component and PC2 was used as the y-component of the PCA-FRF. When damage occurs, the PCA-FRF, particularly the peaks, will shift horizontally away from the undamaged PCA-FRF due to reduction of stiffness. Thus, in this study, the PC1 of the first and second PCA-FRF peaks were extracted and used as the damage sensitive features for the unsupervised-based damage detection method.

2.2 Unsupervised k-means clustering

The general working principle of unsupervised k-means clustering can also be referred to the previously published investigation (Siow *et al*. 2021), where the k-means algorithm is mainly used to evaluate the damage sensitivity of PCA-FRF in an unsupervised manner. As the aim of this study is to use the unsupervised k-means for damage presence detection, a different cluster validation index is used.

There are two main cluster validation methods for unsupervised clustering, which are the internal evaluation and external evaluation methods. The main difference between these two categories is the presence of ground truth labels as a reference. Internal evaluation methods assess the quality of the clusters generated based on the intra-cluster and inter-cluster separation. Some of the internal evaluation indices are Silhouette criterion, Davies-Bouldin, and Dunn's index, which are commonly used to determine the ideal number of clusters for a dataset, i.e., the ideal k for the case of k-means clustering (Liu *et al*. 2022).

External evaluation methods compare the clustering results with the actual partitioning of the samples. Some works applied external evaluation methods to compare the clustering performance of different unsupervised algorithms (Zhu *et al*. 2019), while other works applied them to judge the overall performance of the clustering algorithm based on the actual data distribution with ground truth labels (Tran *et al*. 2019). Examples of these methods are rand index, F-measure, and confusion matrix. In general, the selection of the cluster validation method is highly dependent on the objective of clustering.

For this study, the unsupervised k-means algorithm was used to detect damage presence. Using the undamaged data as the baseline cluster, any outliers would be considered as damaged data. Taking k equals 2, well-clustered results indicate damage presence. As we do not know the actual health status of the incoming data, an internal evaluation index is preferred for clusters' quality evaluation each time a new data comes in. Dunn's index, D was applied to evaluate the clusters generated, which uses Eq. (1) as shown below

$$D = \frac{d'_{min}}{d_{max}} \tag{1}$$

where d'_{min} represents the minimum inter-cluster distance, and d_{max} represents the maximum intra-cluster distance. The higher the value of the Dunn's index, the greater the separation of the clusters and the higher the compactness of the clusters. Therefore, higher Dunn's index value indicates better quality of the two clusters generated, indicating higher possibility of damage presence.

For the proposed scheme, a baseline cluster is built initially. Ideally, the Dunn's index should be low for undamaged conditions and high for damaged conditions, where there will be two distinct clusters when damage occurs. This scenario is only possible if a damage-sensitive feature is used for clustering. Therefore, the PCA-FRF peak was used as the input feature for unsupervised k-means clustering in this study, as its damage sensitivity was proven to be good in the previous study (Siow *et al*. 2021).

2.3 Artificial Neural Network (ANN)

Artificial Neural Network (ANN) is widely used in pattern recognition and classification. Its generalization capability enables the modelling of non-linear relationships and incomplete information, thus suitable in detecting structural damage. The three layers of an ANN model are the input, hidden, and output layer. The number of neurons in each layer is user-defined. In the hidden layer, each neuron sums up the input nodes with different weightings. The summed weightings, x are then transferred to an activation function to generate the output values, $f(x)$. Some of the activation functions are sigmoid, hyperbolic tangent, and linear. For this study, the LeCun's tanh function as shown in Eq. (2) below was used. Let $f(x)$ represent the output value at each individual output node

$$f(x) = 1.716\ tanh(0.667x) \tag{2}$$

where -1$\leq x \leq$ 1, so that the range of $f(x)$ is

$$-1 \lessapprox f(x) \lessapprox 1 \tag{3}$$

For this study, there were four output nodes in the output layer, which correspond to the four plate edges. To compute the damage probability, $f(x)_{normalized}$ for each individual edge (each output node), $f(x)$ is then normalized using Eq. (4) to reduce the range of the output value by half and to shift the midpoint from 0 to 0.5.

$$f(x)_{normalized} = 0.5f(x) + 0.5 \tag{4}$$

Thus, the range of the damage probability, $f(x)_{normalized}$ is

$$0 \lessapprox f(x)_{normalized} \lessapprox 1 \tag{5}$$

It is noted that the damage probability, $f(x)_{normalized}$ is computed for each individual edge. Therefore, the summation of the four damage probabilities shall not be equal to 1.

For this study, the classification threshold for the damage probability value, $f(x)_{normalized}$ was set at 0.4 for single and multiple damages classification. The threshold is user-defined and can be set to any values. As this study aims to predict early damage and multiple damages which are using new and unseen data, where the mode shape differences could be less sensitive, the threshold was set at 0.4. Let Z be the final output value of the output node, and the threshold for $f(x)_{normalized}$ as 0.4, the trained model decides whether the individual edge is damaged or undamaged based on the following conditional statements:

If $f(x)_{normalized} \geq 0.4$,
then predict Z = 1 (Damaged edge)
If $f(x)_{normalized} < 0.4$,
then predict Z = 0 (Undamaged edge)

A feed-forward backpropagation (FFBP) network was used in this work as it is commonly used in damage identification works (Bandara *et al*. 2014, Chen *et al*. 2020a, Mousavi *et al*. 2021). The signals in the feed-forward neural network flow from the input layer to the hidden layer and to the output layer. The backpropagation algorithm was used in this study as it is a popular training algorithm for feed-forward neural network, where the weights are adjusted to minimize the error. Training is stopped based on the stopping criteria i.e., training mean squared error (MSE), training epochs, and validation MSE to avoid overfitting. The validation and classification accuracy of the trained ANN model, n were then calculated using Eq. (6) as shown below

$$n = \frac{\text{number of correctly identified testing samples}}{\text{number of all testing samples}} \times 100\% \tag{6}$$

For this study, as the focus is on identifying support-related damages, the mode shape difference of the four edges were used as the input features of the ANN model for damage localization. The first two mode shapes were used. The mode shape difference is calculated using Eq. (7) as shown below

$$\text{Mode shape difference} = MSV_{Damaged} - MSV_{Undamaged} \tag{7}$$

where MSV is the absolute mode shape value. Acknowledging the fact that mode shape difference is more damage sensitive for higher number of degree freedoms, the authors wish to highlight that rigid body modes of the plate, i.e., heaving and rolling were used instead of elastic modes for this study. The elastic modes, which are of higher order, will certainly require higher degree of freedoms or denser measurement points for better representation of the actual mode shapes. For this study, as rigid body modes were used, the motions are much more predictable, where the nearby points are more likely to move in phase to each other. Thus, using the mode shape differences of the four edges of the plate is considered sufficient.

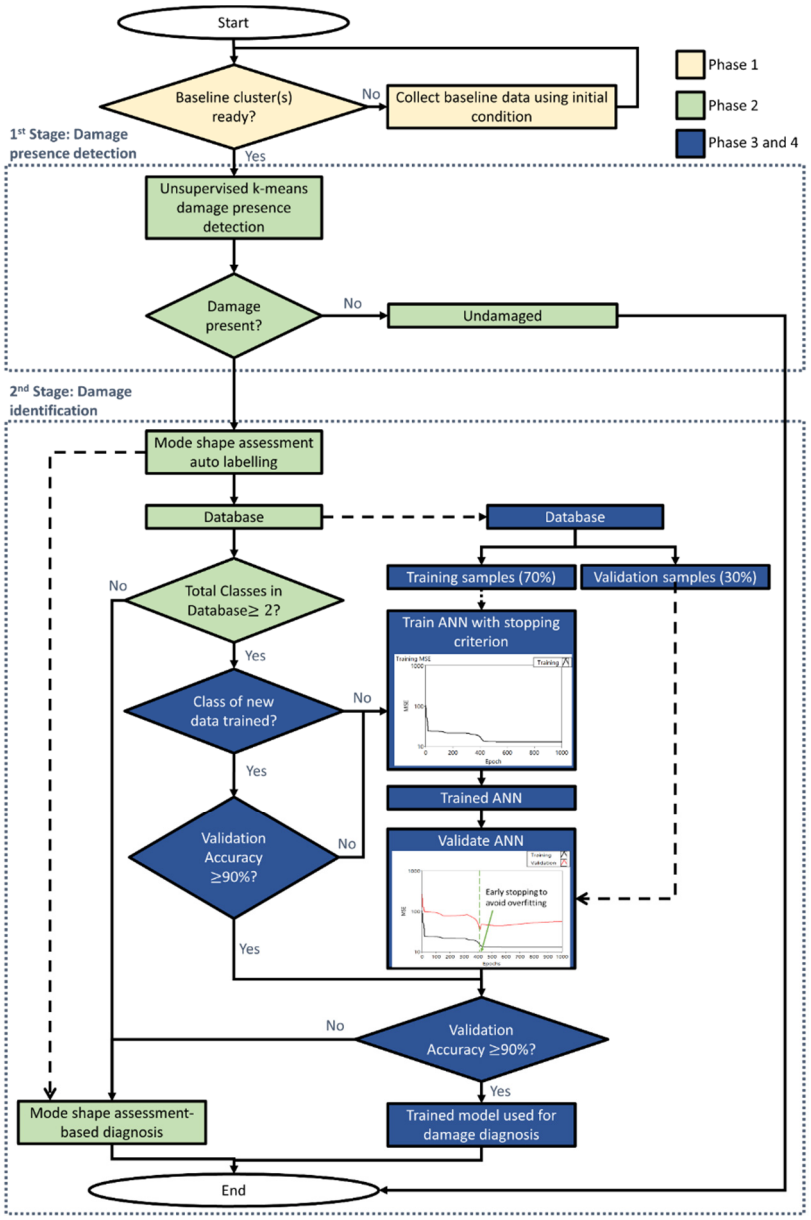

Fig. 1 Flowchart of the two-stage hybrid machine learning damage detection scheme

3. Methods

3.1 The proposed two-stage hybrid machine learning damage detection scheme

Fig. 1 shows the overall flowchart of the proposed damage scheme. In general, the scheme can be divided into two stages, i.e., the first stage detects damage presence, and the second stage identifies the damages. The first stage is initiated once the baseline data is collected. In the first stage, unsupervised k-means clustering is applied to detect damage presence. When outliers of the baseline cluster are detected, the structure is considered damaged. The second stage, i.e., the damage identification stage, will only be initiated when damage is detected in the first stage.

The second stage starts with mode shape assessment to auto label the damaged data using the first mode shape difference. The edge with the largest first mode shape difference is identified as the damage location, and the damaged data is auto labelled with the corresponding edge number. The labelled damaged data is then stored in the database.

A database screening process is then conducted to determine the damage identification method in the second stage of the scheme, which is either the mode shape assessment-based diagnosis or the supervised model-based damage diagnosis method. The mode shape assessment-based diagnosis method identifies the damaged edge based on the largest first mode shape difference to overcome the cold-start and manual labelling issue, whereas the supervised model-based damage diagnosis method identifies the damages based on the prediction generated by a trained ANN model to predict potential multiple damages. When the training database has less than two classes of damage, mode shape assessment-based diagnosis is initiated. The identified damaged edge through mode shape

assessment is used to auto label the damage sample.

When the training database has at least two classes of damage, the scheme will then evaluate the trained model to decide whether to use the supervised model-based damage diagnosis method. Once there are at least two damage classes in the database, supervised model training will be initiated. The database will be divided into 70% training samples and 30% validation samples whenever a new labelled data is added. Training is initiated and stopped when it meets either one of the stopping criteria. The trained model is then tested with the validation samples. The trained model with the epoch just before the validation accuracy rises is selected to avoid overfitting. The selected trained model will be used for supervised-based diagnosis if its validation accuracy is at least 90%. The trained model will also be used for the next damage occurrence given that the damage class is trained to minimize the overall computational power required for model updating. If the validation accuracy is lower than 90%, the model will need to be retrained when the next damage occurrence happens. This also means that the new labelled damage data will be added into the database for model retraining.

In actual scenario, the proposed damage scheme will "grow" and have some transitions as the database grows over the measurement period. Fig. 2 describes how the damage scheme transitions based on four phases, where the scheme starts with Phase 1 and grows towards Phase 4. For Phase 1, 10 undamaged samples, which are collected on the same day, are used to initialize the baseline clusters. The Dunn's index values of the first two PCA-FRF peaks are obtained and used as the baseline values, specifically Baseline 1 for the first peak and Baseline 2 for the second peak. For this study, the sample is an outlier when it shows an increase in Dunn's Index of at least 10% of deviation from either of the baseline values, which considers the structure to be damaged. The percentage deviation from the baseline N was calculated Eq. (8) as shown below

$$\text{Percentage deviation from baseline } N = \frac{\text{Dunn index of Peak } N - \text{Baseline } N}{\text{Baseline } N} \times 100\% \quad (8)$$

where N refers to the PCA-FRF peak number.

The scheme then enters Phase 2 after initialization, meaning that it is ready to conduct damage diagnosis. Mode shape assessment is applied to auto-label and diagnose the damage at Phase 2. Supervised training starts once there is more than one type of damage in the database. The trained model will eventually replace the mode shape assessment for diagnosis at later phases, where more samples and classes are trained, and the validation accuracy is at least 90%. The results for each phase will be explained in the next section.

A series of studies were conducted by comparing the performance of different ANN architectures. The training algorithm, activation function, number of hidden layers and neurons were altered to determine the ANN model with the best performance. For this study, five neurons were used in the hidden layer. The first and second mode shape difference values of the four edges were used as the ANN input features. Thus, the input size of the network was 8. Training is first stopped when it has met either one of the following stopping criteria

1. Training MSE = 1E-05
2. Delta Training MSE = 1E-08
3. Epochs = 500

Considering the average size of the training dataset and the relatively straightforward relationship between the data with damage, training is stopped at 500 epochs even if the first two criteria are not met to avoid overfitting, which can affect the generalization of the model in predicting new samples. The trained model with the epoch just before the validation accuracy rises is then selected to avoid overfitting. The selected trained model will be used for supervised-based diagnosis if its validation accuracy is at least 90%.

3.2 *Experimental setup*

As this study is a continuation of a previous investigation (Siow *et al*. 2021), similar experimental setup and case study were used. Fig. 3 shows the experiment setup and Fig. 4 shows the measurement points, impact direction and location for modal analysis, and damage locations of the test plate for this study.

Phase	Phase 1: Initialization	Phase 2: Diagnosis using unsupervised k-means and mode shape assessment	Phase 3: Diagnosis using unsupervised k-means and mode shape assessment/ trained supervised model	Phase 4: Diagnosis using unsupervised k-means and trained supervised Model
Status	• Number of classes in database: 0 • No trained model available	• Number of classes in database: 0 or 1 • No trained model available	• Number of classes in database: Equal or more than 2 • Trained model available, depending on the validation accuracy	• Number of classes in database: Equals to the number of supports • Trained model available with validation accuracy of at least 90%
Features	• Modal parameter extraction • PCA • Unsupervised k-means	• Modal parameter extraction • PCA • Unsupervised k-means • Mode shape assessment (auto label and diagnose)	• Modal parameter extraction • PCA • Unsupervised k-means • Mode shape assessment (auto label and diagnose)/ Supervised ANN model (diagnose)	• Modal parameter extraction • PCA • Unsupervised k-means • Mode shape assessment (auto label) • Supervised ANN model

Fig. 2 Transitions and status of the proposed damage scheme according to phase

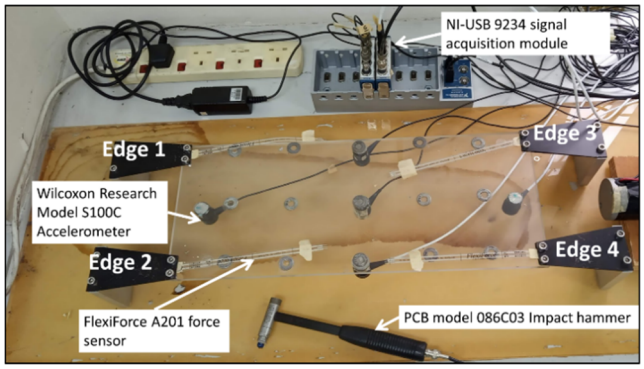

Fig. 3 Experimental setup (Siow *et al*. 2021)

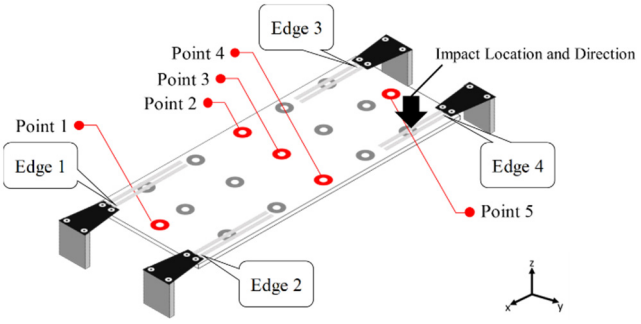

Fig. 4 Measurement points, impact, and damage locations of the test rig

To demonstrate the performance of the scheme at Phase 3 to 4, the number of damaged samples and classes (damage locations) in the database was increased gradually. For each damage location, different high severity conditions (DL4 – DL6) were simulated by loosening or removing the screws. The database randomly splits into 70% training data and 30% validation data whenever a new data is added. The model is then trained with the 70% training data and tested with the 30% validation data. The trained model will only be used to identify potential multiple damages if the validation accuracy surpasses the 90% benchmark.

The total number of damaged samples for each damage location was 30 samples for this study. Thus, the final trained model for this study had a total of 120 damaged samples in the database. Similarly, the database was then split into 70% training data and 30% validation data. Training and testing using the validation data was then initiated. At this stage, unseen early single damage cases and multiple damages were used to test the final trained model. For the early or low severity single damage cases (DL1 – DL3), different conditions were simulated by slightly loosening the screws at each of the damage locations. A total of 30 early single damage samples were collected at each of the damage location. For the multiple damages, a total of 60 samples were collected.

4. Results and discussion

4.1 Phase 1: Initialization

For Phase 1, 10 undamaged samples were acquired to initialize the baseline cluster. Fig. 5 shows the FRFs and PCA-FRF of the undamaged condition. Based on Fig. 5, it is observed that the PCA-FRF resembles the outline of the original FRFs, where the important features, i.e., resonance

Table 1 List of simulated undamaged, single damage (Siow *et al*. 2021) and multiple damages with descriptions

Condition	Damage severity	Description	Damage location(s)
Undamaged	DL0	Screws of all edges were tightened at 150 N	None
Single damage	DL1	Screws at damaged edge were loosened to 113 N, others remained at 150 N	• Edge 1 • Edge 2 • Edge 3 • Edge 4
	DL2	Screws at damaged edge were loosened to 75 N, others remained at 150 N	
	DL3	Screws at damaged edge were loosened to 38 N, others remained at 150 N	
	DL4	Screws at damaged edge were loosened to 0 N, others remained at 150 N	
	DL5	At damaged edge, one screw was loosened to 0 N, the other screw was removed. Others remained at 150 N	
	DL6	At damaged edge, both screws were removed. Others remained at 150 N	
Multiple damages	DL4	Screws at damaged edges were loosened to 0 N, others remained at 150 N	• Edge 1 and 2 • Edge 1 and 3 • Edge 1 and 4 • Edge 2 and 3 • Edge 2 and 4 • Edge 3 and 4

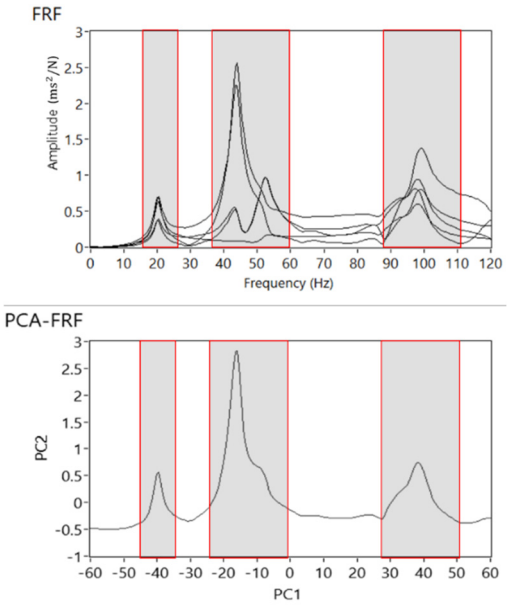

Fig. 5 FRFs and PCA-FRFs of the undamaged condition; The peaks of the FRFs and PCA-FRF are highlighted

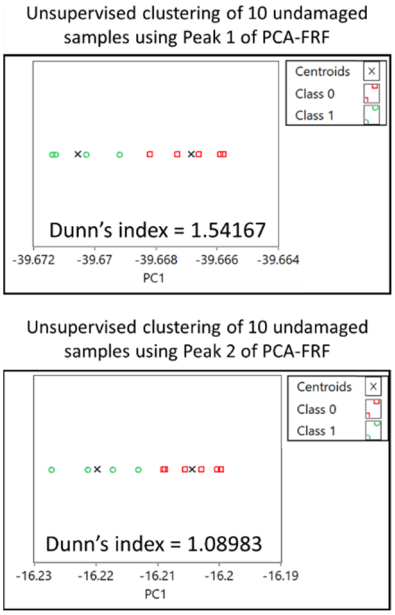

Fig. 6 Unsupervised k-means clustering results for the Peak 1 and Peak 2 of the PCA-FRF for initialization phase

peaks, were retained in the PCA-FRF. This shows that the PCA-FRF can represent the FRFs in a lower dimension yet retaining the important features of the FRFs.

The scheme starts with building a baseline cluster using the undamaged samples. Fig. 6 shows the Dunn's Index and the clustering results of the 10 undamaged samples. The PC1 of the first two PCA-FRF peaks were used as the clustering features since damage due to stiffness reduction can be represented by horizontal FRF shift. Using k equals 2, the Dunn's index for the initialization clustering result was 1.54167 for the first peak, and 1.08983 for the second peak. Since there was no damage occurred yet, the dynamic

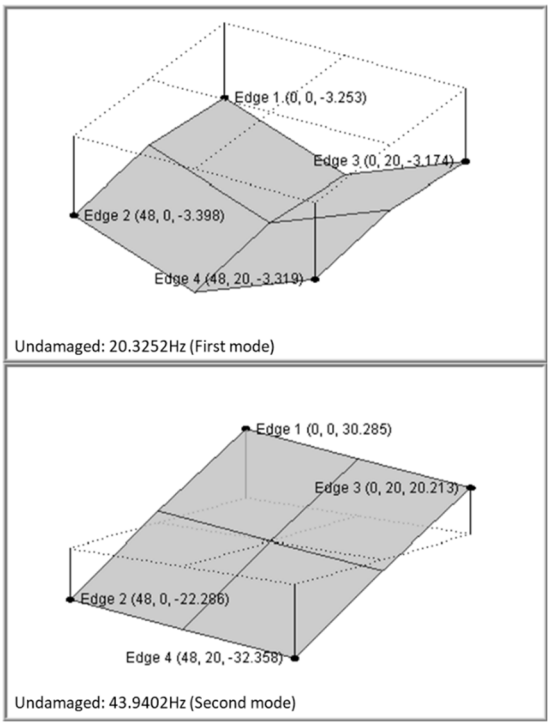

Fig. 7 First mode shape and second mode shape of the undamaged condition. The first mode is a heaving mode, and the second mode is a rolling mode

behavior of the plate structure remained unchanged. Thus, the PCA-FRF peaks obtained showed zero to insignificant deviations, which led to the low Dunn's index values indicating poor clustering results. As there is no standard value for a good clustering result, the Dunn's index values during the initialization phase were used as the baseline or reference values, where 10% deviation or more from the baseline Dunn's index considered the structure as damaged for this study. The first and second mode shapes were also extracted as shown in Fig. 7 The (x, y, z) vector of the four edges were labeled. For this study, the vertical deflection was focused. Hence, the z-vector shown was the mode shape value. Based on Fig. 7, the first mode shape is a heaving mode, where all points are moving in phase to each other. The second mode shape is a rolling mode, where the pairs Edge 1 and 3 and pairs Edge 2 and 4 are moving out of phase to each other.

4.2 Phase 2: Diagnosis using unsupervised k-means and mode shape assessment

After the baseline cluster was initialized, the damage scheme was transitioned to Phase 2, i.e., diagnosis using unsupervised k-means and mode shape assessment. The first condition simulated for this study was an undamaged condition to demonstrate how the scheme reacts when the structure is still healthy. Fig. 8 shows the clustering results and the corresponding Dunn's indices. It is noted that the Dunn's index for the first two peaks were updated to 1.60417 and 1.11253, which deviated by 4.1% and 2.1% respectively from the baseline values. As the deviation was below the 10% threshold, the structure was detected as

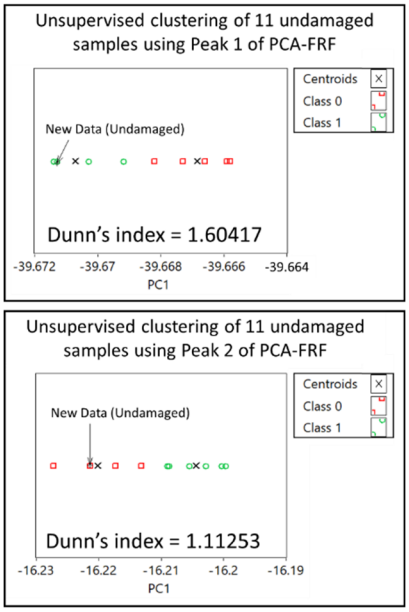

Fig. 8 Clustering result of the Peak 1 and Peak 2 of the PCA-FRF with the corresponding Dunn's index of Undamaged.

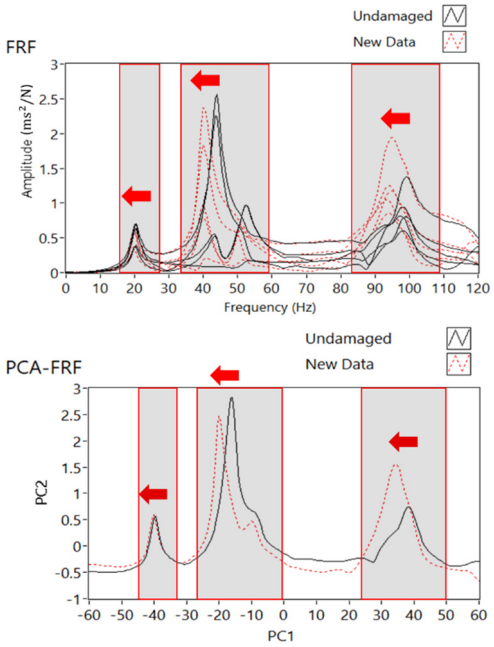

Fig. 9 Overlaid FRFs and PCA-FRFs of undamaged and DL4 at Edge 1. The red dotted curves and arrows represented the damage curves and the shift of peaks due to damage

"undamaged". The PC1 of the first two peaks were added into the undamaged clusters.

The second condition simulated was a single damage case, i.e., DL4 at Edge 1 to demonstrate how the scheme reacts to the first observed damage. Fig. 9 shows the overlaid FRFs and PCA-FRF of the damage case with the undamaged condition. When damage occurs, it is observed that the FRFs shifted horizontally away from the

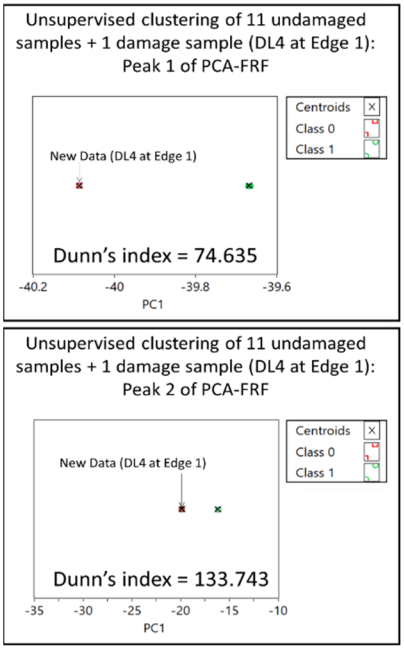

Fig. 10 Clustering result of the Peak 1 and Peak 2 of the PCA-FRF with the corresponding Dunn's index of Undamaged

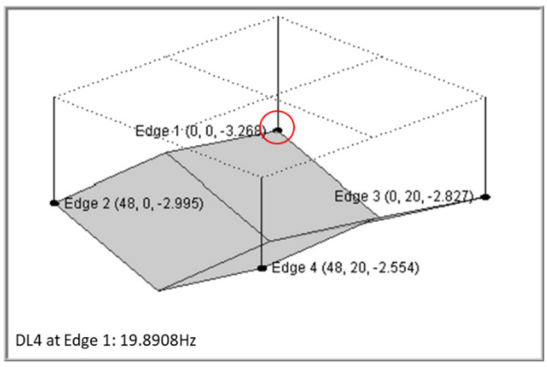

Fig. 11 First mode shape of DL4 at Edge 1. The dotted lines represent the undeformed plane

undamaged FRFs, which indicates the reduction of stiffness of the structure. The horizontal shift due to damage is also observed for the PCA-FRF. It is also shown that the shift of the PCA-FRF due to damage is more easily shown compared to the FRFs, where the shift of PCA-FRF peaks can be directly measured. Fig. 10 then shows the clustering results and the corresponding Dunn's index for the single damage case. The Dunn's index for the first two peaks were updated to 74.6375 and 133.743, where both deviated by more than 10% from the baseline Dunn's index. Thus, the structure was detected as "damaged". The PC1 of the peak was not remained in the clustering plot, leaving only the undamaged cluster in the plot for the next diagnosis.

Since damage presence was detected, the second stage, i.e., mode shape assessment using the first mode shape was initiated for damage identification. Fig. 11 shows the first mode shape of the damage case. From the mode shape values, it is noted that the damaged edge shows the largest

Table 2 Dunn's Index of the clustering results using 1st and 2nd PCA-FRF peaks for all cases

Damage severity	Damage location	Dunn's index of 1st Peak	Dunn's index of 2nd Peak
DL0	Undamaged (Baseline)	1.54167	1.08983
	Undamaged	1.60417	1.11253
DL1	Edge 1	12.548	14.263
	Edge 2	13.780	8.437
	Edge 3	0.519	3.252
	Edge 4	1.880	9.390
DL2	Edge 1	24.709	31.444
	Edge 2	47.566	18.215
	Edge 3	3.316	7.513
	Edge 4	1.234	18.786
DL3	Edge 1	42.816	60.444
	Edge 2	71.548	38.324
	Edge 3	17.548	17.470
	Edge 4	9.084	38.684
DL4	Edge 1	74.638	133.743
	Edge 2	137.620	99.659
	Edge 3	80.852	95.586
	Edge 4	95.941	240.383
	Edge 1 and 2	317.655	272.51
	Edge 1 and 3	221.334	229.663
	Edge 1 and 4	155.566	402.201
	Edge 2 and 3	207.066	316.935
	Edge 2 and 4	206.191	209.484
	Edge 3 and 4	181.495	196.855
DL5	Edge 1	92.370	165.066
	Edge 2	164.941	156.383
	Edge 3	126.137	180.855
	Edge 4	100.316	216.895
DL6	Edge 1	726.191	368.757
	Edge 2	866.405	337.833
	Edge 3	781.941	379.495
	Edge 4	644.673	403.390

Table 3 First mode shape difference and assigned label for all damage cases

Damage severity	Damage location	Mode shape difference				Labeled as
		Edge 1	Edge 2	Edge 3	Edge 4	
DL1	Edge 1	0.031	-0.042	-0.005	-0.077	1
	Edge 2	-0.199	-0.058	-0.237	-0.095	2
	Edge 3	-0.087	-0.056	-0.074	-0.043	4
	Edge 4	-0.069	-0.017	-0.070	-0.018	2
DL2	Edge 1	-0.081	-0.150	-0.149	-0.218	1
	Edge 2	-0.152	0.065	-0.350	-0.132	2
	Edge 3	-0.043	-0.045	-0.022	-0.024	3
	Edge 4	-0.104	-0.041	-0.084	-0.022	4
DL3	Edge 1	-0.097	-0.224	-0.186	-0.313	1
	Edge 2	-0.098	0.213	-0.443	-0.132	2
	Edge 3	-0.064	-0.122	-0.009	-0.067	3
	Edge 4	-0.093	-0.003	-0.010	0.080	4
DL4	Edge 1	0.015	-0.403	-0.347	-0.765	1
	Edge 2	-0.012	0.400	-0.616	-0.204	2
	Edge 3	-0.150	-0.456	0.118	-0.188	3
	Edge 4	-0.242	0.362	0.420	1.023	4
DL5	Edge 1	-0.265	-0.490	-0.448	-0.673	1
	Edge 2	-0.006	0.540	-0.669	-0.122	2
	Edge 3	-0.272	-0.978	0.436	-0.270	3
	Edge 4	-0.213	0.454	0.536	1.203	4
DL6	Edge 1	-0.764	-1.693	-1.173	-2.102	1
	Edge 2	-0.711	1.139	-2.024	-0.174	2
	Edge 3	-0.801	-2.472	0.967	-0.705	3
	Edge 4	-1.301	2.417	1.745	5.463	4
DL4	Edge 1 Edge 2	0.026	0.453	-0.623	-0.196	2
	Edge 1 Edge 3	-0.105	-0.896	-0.003	-0.794	3
	Edge 1 Edge 4	0.038	0.374	0.317	0.652	4
	Edge 2 Edge 3	-0.318	-0.581	-0.204	-0.467	3
	Edge 2 Edge 4	-0.060	0.634	-0.341	0.353	2
	Edge 3 Edge 4	-0.283	-0.256	0.470	0.497	4

mode shape value among the four edges, indicating that the plate deflects towards the damaged edge at Mode 1. It is also noted that Edge 1 shows the largest mode shape difference, which indicates that Edge 1 has deflected away the most from the undeformed plane, whereas the other three edges showed negative mode shape difference, indicating the three edges have "moved nearer" to the undeformed plane at Mode 1. As a result, the plate shows a deflect-towards-damage movement at Mode 1. Based on the edge with the largest mode shape difference, the case was identified as damage at Edge 1. The identified damage location, i.e., 1, also serves as the data label. The labelled data was then stored in a database for future model training. Thus, this shows how the mode shape-based diagnosis overcomes the manual labelling and cold start issue when there is no trained model available yet.

Other damage cases that were listed in Table 1 were also simulated for this study to demonstrate the performance of the scheme on other damage cases in Phase 2. Table 2 shows the Dunn's index of the first and second PCA-FRF peaks, and Fig. 12 shows the percentage deviation of the

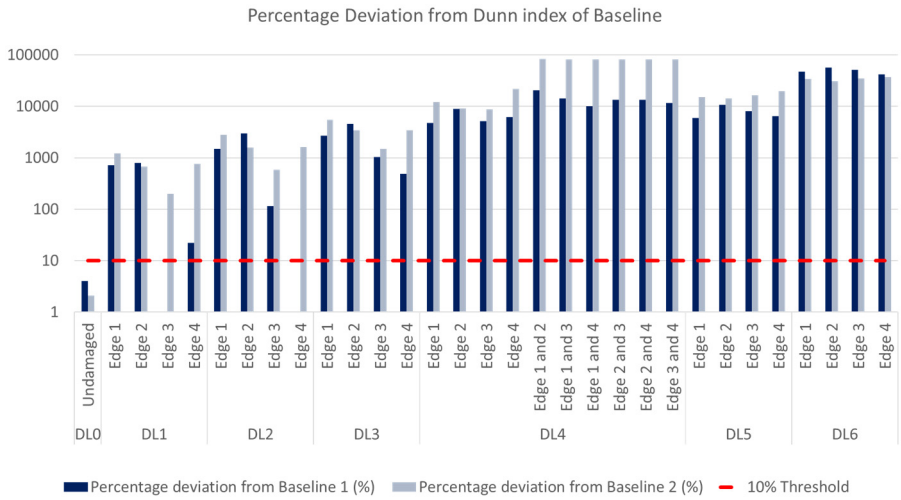

Fig. 12 Percentage deviation of the 1st and 2nd PCA-FRF peaks from Baseline 1 and Baseline 2 for all cases. Cases with negative percentage deviation are shown as zero in this logarithmic-scale chart.

first two peaks from the baseline values for all damage cases. Overall, the Dunn's index exceeded the baseline value by more than the threshold of 10%, indicating that damage presence can be detected in general. It is noted that the Dunn's index of the first peaks of damage cases DL1 at Edge 3 and DL2 at Edge 4 were 0.519 and 1.234 based on Table 2, which showed a reduction of 66.3% and 19.9% from Baseline 1. This could be due to their low damage severity, thus reducing the overall damage sensitivity. However, the Dunn's index of the second peaks for the two damage cases exceeded Baseline 2 by more than 10%. Still, taking the overall PCA-FRF shift for damage detection, damage presence was detected for the two low severity single damage cases as the second PCA-FRF peaks showed well-clustered results. Therefore, this shows that the first stage of the scheme is feasible in detecting damage presence even for light damage.

The second stage was initiated since damage presence was detected at the first stage for all damage cases. Mode shape assessment-based diagnosis was applied in this phase. Table 3 shows the first mode shape difference for all the damage cases tested. Overall, most of the damage cases showed the deflect-towards-damage movement at Mode 1. For single damage cases, damage was correctly identified for all damage cases except for two low severity cases, i.e., DL1 at Edge 3 and DL1 at Edge 4. As for all the multiple damage cases tested, at least one of the damaged edges was correctly identified. Therefore, assuming that it is accurate when one of the damaged edges is correctly identified for the multiple damage cases, the overall accuracy of mode shape assessment using first mode shape for diagnosis was 93.3%, which is acceptable when there are no past damaged events available as a reference at this phase. Hence, this shows that the mode shape assessment-based diagnosis using the first mode shape is not only feasible for damage identification when there is no trained model available yet, but also automates the data labelling process before supervised model training.

4.3 Phase 3: Diagnosis using unsupervised k-means and mode shape assessment/ supervised model

Once the database has two classes of damage, the scheme enters Phase 3. Each time a new data is added to the database, the database will randomly split into 70% training data and 30% validation data. ANN model training is initiated if the new data is a new damage class (damage location). The trained model will then be used damage identification, i.e., single and multiple damages if the validation accuracy is at least 90%. Otherwise, mode shape assessment-based diagnosis would be initiated, where the damage location is identified based on the first mode shape difference. As the ANN model has four output nodes that correspond to the four plate edges, the normalized output values at each output node indicates the damage probability of the individual corresponding edge. For each individual edge, the damage probability range is between 0 to 1, in which 1 indicates the highest damage probability. The trained model identifies the individual edge as damaged when the damage probability is at least 0.4. Thus, this allows the trained model to identify both single and multiple damages. For the multiple damage classification accuracy, partially correct classification is considered. This section demonstrates how the single (validation) and multiple damages classification accuracy improves when the number of samples and classes increases over time.

Fig. 13 shows the performance of the trained models, where the number of samples and classes trained were increased gradually, starting from Trained Model 1 with only 1 sample of class "1" and "2". Overall, both validation and multiple damages classification accuracy improved as the number of training classes increased and when the dataset was balanced. For multiple damages, in general, at least one of the damaged edges can be correctly identified, given that the damage class was trained. It is assumed that Trained Model 1 was produced at the beginning of Phase 3. Based on Fig. 13, the overall validation accuracy was 100% using Trained Model 1, indicating that the trained model

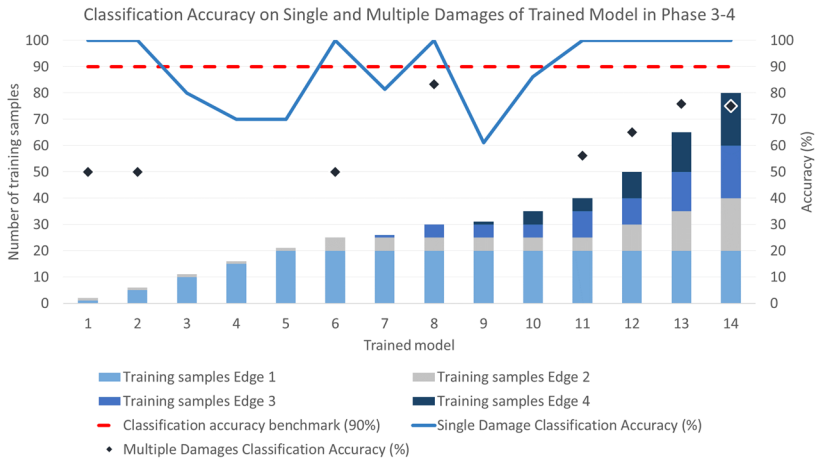

Fig. 13 Classification accuracy of trained model in Phase 3 to 4

can identify single damage at Edge 1 and Edge 2 with good accuracy. As it has exceeded the 90% benchmark, Trained Model 1 was also used to identify potential multiple damages (Edge 1 and 2). However, it is found that Trained Model 1 can only identify them as single damage where only one of the damaged edges was identified, thus showing 50% accuracy for multiple damage identification.

Assuming the following 19 damage occurrences were an Edge 1 damage, and the model was retrained upon entry of each new damage data. Due to dataset imbalance, the overall validation accuracy dropped from 100% to 70% when there were more class "1" samples trained compared to class "2" samples as shown in Trained Models 2, 3, 4, and 5. Thus, supervised model-based diagnosis was not applied to identify multiple damages for Trained Models 3, 4, and 5 as the validation accuracy did not meet the 90% benchmark. When more class "2" samples were trained, the validation accuracy returned to 100%. However, the multiple damages identification remained 50%. This shows that a high imbalance dataset could reduce the overall validation accuracy and thus, reduces the probability of using the supervised model-based diagnosis in the second stage of the damage scheme.

An Edge 3 damage was then simulated and detected by the scheme. Thus, supervised training was initiated and produced Trained Model 7. Based on Fig. 13, it is noted that upon the addition of a class "3" sample, the validation accuracy dropped from 100% to 81.5%. It improved to 100% when more class "3" samples were trained as shown in Trained Model 8. When Trained Model 8 was applied to identify multiple damages (Edge 1 and 2; Edge 1 and 3; Edge 2 and 3), the overall accuracy was 83.3%. It is noted that the identification of multiple damages Edge 1 and 2 improved when three damage classes were trained, which shows the possibility of improved generalization performance due to the addition of new training classes. An Edge 4 damage was then simulated and detected by the scheme. Training occurred and Trained Model 9 was produced. Based on the graph, it is shown that the validation accuracy dropped to 61.1% but improved gradually and became more consistent when of the dataset became more balanced, where samples of Edge 2, 3, and 4 were gradually added in Trained Model 10 to 14. For Trained Model 11 to 14, the multiple damages classification accuracy improved and peaked at 75% as the training samples increases. Based on Trained Model 11 and 12, the improvement of the multiple damages classification accuracy was observed when the dataset becomes more balanced in Trained Model 12. Therefore, in general, the overall classification accuracy improved when the dataset was balanced and more classes were trained.

4.4 Phase 4: Diagnosis using unsupervised k-means and supervised model

The damage scheme was at Phase 4 when damage samples of all four supports were collected for this study, and the validation accuracy was at least 90%. Trained Model 14 was found to have a validation accuracy of 100%, surpassing the 90% benchmark, thus eligible to identify potential multiple damages. Since it was found that the validation accuracy of the 4-class trained models in Fig. 13 i.e., Trained Model 12, 13 and 14 maintained above the 90% benchmark, the authors assumed that Trained Model 14 could be "matured" enough to demonstrate Phase 4, where the second-stage diagnosis was made fully by the trained supervised model. Therefore, Trained Model 14 was tested with unseen early single damage cases and multiple damages to assess its performance on unseen or untrained damage cases. The performance of Trained Model 14 on unseen damage cases were discussed in this section.

Fig. 14 shows the performance of Trained Model 14 in identifying unseen early single damage cases which is presented in a confusion matrix. It is noted that 75% of the total low severity damage samples can be accurately classified, where low severity single damage at Edge 1 and Edge 3, which are located away from the impact location, can be accurately identified. In general, Trained Model 14 can diagnose unseen early damage (DL1 to DL3) with an acceptable accuracy although their mode shape differences are smaller than the trained DL4 to DL6 single damage cases.

Fig. 15(a) shows the predicted damage probabilities of the four edges for one sample from each of the multiple

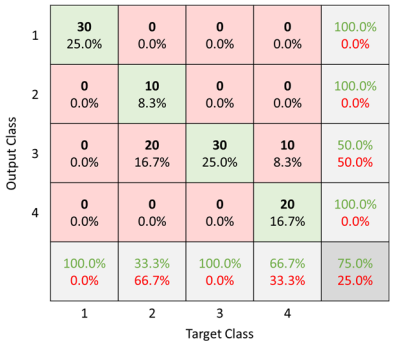

Fig. 14 Confusion matrix of low severity (DL1 – DL3) single damage cases

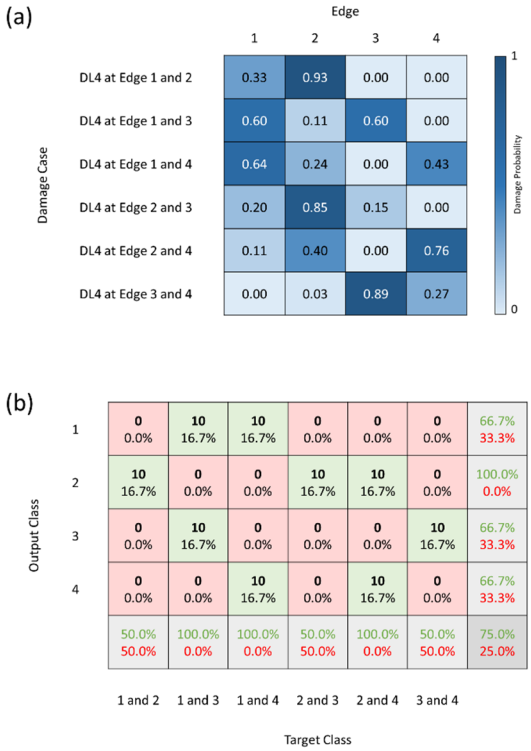

Fig. 15 (a) Predicted damage probabilities at each of the individual edges for the multiple damage cases; (b) Confusion matrix of multiple damage cases

damage cases and Fig. 15(b) shows the confusion matrix for all multiple damage cases. Six different multiple damage cases were used to test the trained model, where each multiple damage case consists of ten samples. Based on Fig. 15(a), it is noted that for all the multiple damage cases tested, at least one of the damaged edges was identified with a damage probability of at least 0.4, thus showing that the first two mode shapes are damage sensitive in general. Fig. 15(b) summarizes the performance of Trained Model 14 in identifying unseen multiple damages. It is noted that the overall accuracy in predicting multiple damages is 75%, where partially correct classification is considered and measured as 50% accurate.

For this study, the multiple damage cases can be categorized into two groups, i.e., same-sided damages and diagonal damages. Damage at Edge 1 and 4 and Damage at Edge 2 and 3 are named as diagonal damages because the damaged edges are faced diagonally to each other, whereas the other multiple damage cases are named as same-sided damages. Fig. 16 and Fig. 17 show the first and second mode shapes for the multiple damage cases, and Table 4 shows the first two mode shape differences of the multiple damage cases. Overall, it is observed that the first mode shapes are more sensitive to the same-sided damages, and the second mode shapes are more sensitive to the diagonal damages. The plate deflects towards same-sided damages at Mode 1 (heaving mode) and deflects towards the diagonal damages at Mode 2 (rolling mode). Based on the mode shape differences, it is found that the same-sided damages can be correctly identified using the heaving mode, whereas the diagonal damages can be correctly identified using the rolling mode. The nature of the mode shape itself could affect its damage sensitivity. As the same-sided damages are adjacent to each other, the heaving mode allows the plate to

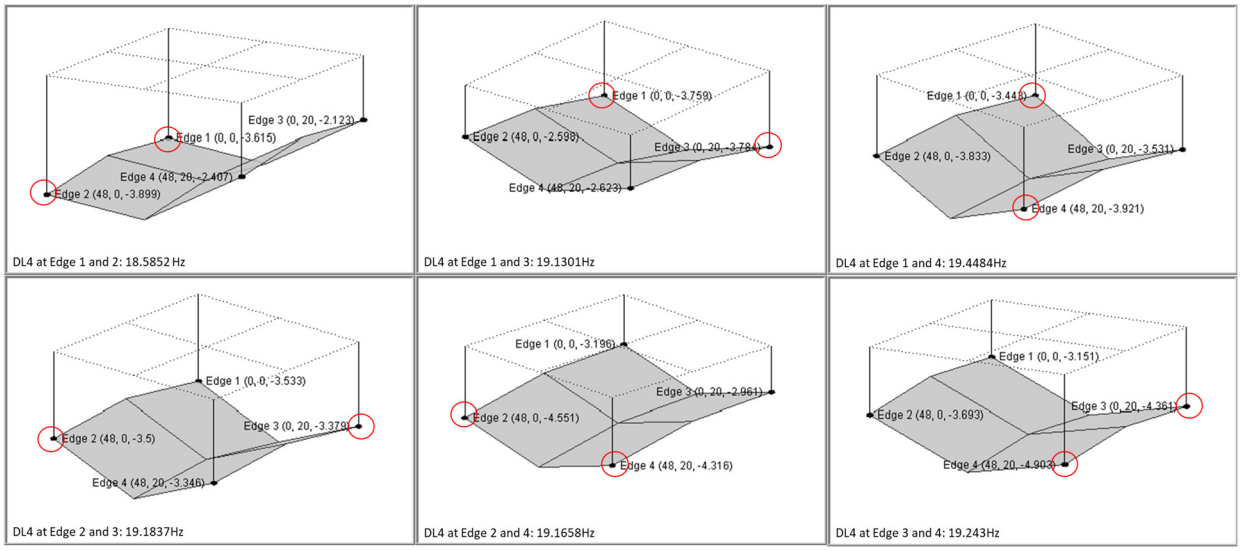

Fig. 16 First mode shapes of the multiple damage cases. The red circle indicates the damaged edge

Table 4 First two mode shape differences of the multiple damage cases

Multiple damages	1st mode shape difference				2nd mode shape difference			
	Edge 1	Edge 2	Edge 3	Edge 4	Edge 1	Edge 2	Edge 3	Edge 4
DL4 at Edge 1 and 2	0.362	0.501	-1.051	-0.912	-13.431	-6.225	-5.764	-13.892
DL4 at Edge 1 and 3	0.506	-0.800	0.610	-0.696	-11.835	-6.587	-4.679	-13.743
DL4 at Edge 1 and 4	0.190	0.435	0.357	0.602	-3.019	-15.177	-15.520	-2.676
DL4 at Edge 2 and 3	0.280	0.102	0.205	0.027	-25.997	-6.695	-5.100	-27.592
DL4 at Edge 2 and 4	-0.057	1.153	-0.213	0.997	-2.290	-5.257	-7.035	-0.512
DL4 at Edge 3 and 4	-0.102	0.295	1.187	1.584	-0.196	-5.286	-6.897	1.415

be easily deflected towards the damaged side, which allows correct identification of the damaged edges. When diagonal damages occur, it could be difficult for the plate to deflect largely at both damaged edges in heaving mode compared to rolling mode. The points of the entire plate are anti-nodes in heaving mode, which makes the change in deflection at the diagonal damaged edges to be less significant. While in rolling mode, the center of the plate is a nodal line with minimum deflection, which makes the plate easier to deflect towards both damaged edges and show greater change in deflection. Therefore, using both mode shapes for supervised model-based diagnosis may reduce the overall damage sensitivity as only one of them is damage sensitive. As a result, the damage probability range of the undamaged and damaged edges could overlap as shown in Fig. 15(a), leading to less accurate identification for the diagonal damages. Therefore, it is acknowledged that mode shape assessment using the more damage sensitive mode shape with a suitable, generalized threshold could improve the proposed method in identifying multiple damages on plate-like structures. It is suggested that for future work, an automated method to select the more damage sensitive mode shape before mode shape assessment should be developed to improve the auto-labeling method, where multiple damages could also be labeled accurately at earlier stages, and thus minimize the overall identification errors.

It is also noted that the case study was conducted with noise-free data, thus, showing near-accurate damage identification. In actual scenario, measured data is more likely to be contaminated with noise, which makes it difficult to obtain a clean FRF for accurate estimation of modal parameters. The sources of noise are not limited to ambient noises but also from rotating parts if the system is in-operation mode, and vibration from nearby operating structures. As a result, the modes that appear are a combination of actual system modes and noise modes. It is worth noting that the system modes or modal parameters will not change due noise presence as they are the global properties which are already inherited. Instead, the noise will cover the actual system modes, making them difficult to be extracted out. Faulty damage detection happens if the noise modes are not distinguished from the actual system modes. There are several established methods developed for this distinguishing procedure, which are mostly in the scope of modal identification algorithms. However, experienced judgement is still often required to use the sorting tools (Bao *et al*. 2015). To effectively apply modal analysis in modal-based damage detection methods, denoising the upstream of the collected data at the first place is much desired. ISMA is an alternative modal analysis method to denoise the FRFs and has shown to be effective in the damage identification application (Chen *et al*. 2020a).

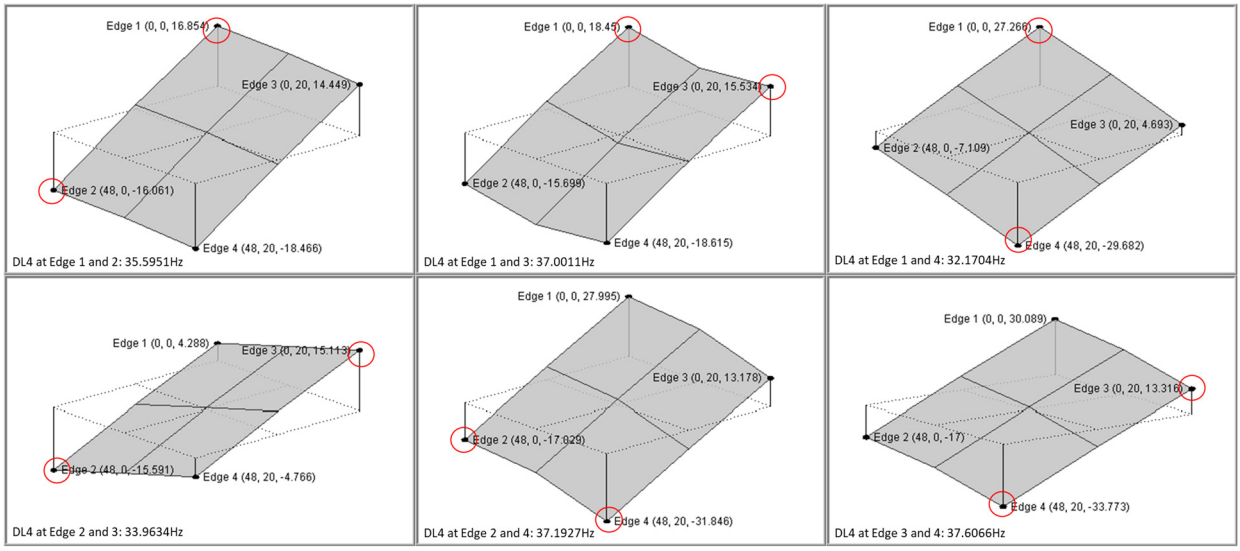

Fig. 17 Second mode shapes of the multiple damage cases. The red circle indicates the damaged edge

As this work focuses on highlighting the hybrid scheme methodology, the actual implementation of the scheme with ISMA would be a work in near future to better validate the practicality of the proposed scheme on structures or systems exposed to noise.

Besides, based on the results in Fig. 15, it is also noted that the damage probability range of the undamaged and damaged edges overlap each other. In other words, the damage probability range of the damaged edges is not narrow enough to be distinguished from the undamaged edges. The authors acknowledged that the results could be further improved by increasing the number of training samples. However, as the accuracy of a supervised learning model highly depends on the samples trained, its extrapolation capacity is limited resulting in low reliability in predicting new or extreme events such as three-sided multiple damages or cracks. Therefore, integrating a physics-based digital twin into a machine learning-based scheme can better improve the sustainability of the overall damage scheme or monitoring scheme, which is a work in progress of the authors.

5. Conclusions

A two-stage hybrid modal-machine learning scheme is proposed to alleviate the cold-start and manual labeling issues faced by ML-based SHM. From the results, it is shown that the first stage, i.e., PCA-FRF-based unsupervised k-means damage detection method is feasible even for light damage. It is acknowledged that other factors such as environmental conditions of the undamaged structure should also be considered when setting the deviation threshold for the clustering-based damage presence detection. This would be considered in our future investigation to further improve the robustness of the proposed method towards environmental changes. It is also observed that generally, the first mode shape is sensitive to single and multiple damages, where the damaged edge shows the largest mode shape difference. Integrating the mode shape assessment-based diagnosis has shown to overcome the cold-start and manual labeling issues, where accurate damage identification is possible even when there is no trained model available yet, and the identified damage can be auto-labeled and stored for future supervised model-training. The single damage-trained ANN model can also identify multiple damages and low severity single damage at an acceptable accuracy. The investigation on an automated method to select the more damage sensitive mode shape before mode shape assessment is considered as a future work to further improve the auto-labeling method for machine learning-based damage assessment schemes and multiple damages identification. Besides, ISMA will be integrated with the proposed scheme for actual implementation as a work in near future to improve the scheme's robustness towards noise. To further improve the sustainability of the scheme, the integration of a physics-based digital twin into the scheme is highly suggested, and it is a work in progress of the authors.

Acknowledgments

The authors wish to acknowledge the financial support and advice given by Impact-Oriented Interdisciplinary Research Grant (IIRG007B-2019), private funding by SD Advance Engineering Sdn Bhd (PV032-2018), Advanced Shock and Vibration Research (ASVR) Group of University of Malaya and other project collaborators.

References

Abdulkareem, M., Bakhary, N., Vafaei, M., Noor, N.M. and Mohamed, R.N. (2019), "Application of two-dimensional wavelet transform to detect damage in steel plate structures", *Measurement*, **146**, 912-923. https://doi.org/10.1016/j.measurement.2019.07.027

Bandara, R.P., Chan, T.H.T. and Thambiratnam, D.P. (2014), "Frequency response function based damage identification using principal component analysis and pattern recognition technique", *Eng. Struct.*, **66**, 116-128. https://doi.org/10.1016/j.engstruct.2014.01.044

Bao, X.X., Li, C.L. and Xiong, C.B. (2015), "Noise elimination algorithm for modal analysis", *Appl. Phys. Lett.*, **107**(4), 5. https://doi.org/10.1063/1.4927642

Bull, L., Worden, K., Manson, G. and Dervilis, N. (2018), "Active learning for semi-supervised structural health monitoring", *J. Sound Vib.*, **437**, 373-388. https://doi.org/10.1016/j.jsv.2018.08.040

Bull, L.A., Rogers, T.J., Wickramarachchi, C., Cross, E.J., Worden, K. and Dervilis, N. (2019), "Probabilistic active learning: An online framework for structural health monitoring", *Mech. Syst. Signal Process.*, **134**, 20. https://doi.org/10.1016/j.ymssp.2019.106294

Cevasco, D., Tautz-Weinert, J., Richmond, M., Sobey, A. and Kolios, A.J. (2022), "A damage detection and location scheme for offshore wind turbine jacket structures based on global modal properties", *ASCE-ASME J. Risk Uncertain. Eng. Syst. Part B-Mech. Eng.*, **8**(2), 12. https://doi.org/10.1115/1.4053659

Chang, C.M., Lin, T.K. and Chang, C.W. (2018), "Applications of neural network models for structural health monitoring based on derived modal properties", *Measurement*, **129**, 457-470. https://doi.org/10.1016/j.measurement.2018.07.051

Chen, S., Ong, Z.C., Lam, W.H., Lim, K.-S. and Lai, K.W. (2020a), "Operational damage identification scheme utilizing de-noised frequency response functions and artificial neural network", *J. Nondestr. Eval.*, **39**(3), 66. https://doi.org/10.1007/s10921-020-00709-x

Chen, S.L., Ong, Z.C., Lam, W.H., Lim, K.S. and Lai, K.W. (2020b), "Unsupervised damage identification scheme using pca-reduced frequency response function and waveform chain code analysis", *Int. J. Struct. Stab. Dyn.*, **20**(8), 26. https://doi.org/10.1142/s0219455420500911

Chen, Y., Zhao, Z.Y., Wu, H.Z., Chen, X., Xiao, Q.B. and Yu, Y.Q. (2022), "P fault anomaly detection of synchronous machine winding based on isolation forest and impulse frequency response analysis", *Measurement*, **188**, 10. https://doi.org/10.1016/j.measurement.2021.110531

Esfandiari, A., Nabiyan, M.S. and Rofooei, F.R. (2020), "Structural damage detection using principal component analysis of frequency response function data", *Struct. Control Health Monit.*, **27**(7), 21. https://doi.org/10.1002/stc.2550

Ghannadi, P. and Kourehli, S.S. (2019), "Data-driven method of damage detection using sparse sensors installation by serepa", *J. Civ. Struct. Health Monit.*, **9**(4), 459-475.

https://doi.org/10.1007/s13349-019-00345-8
Janeliukstis, R., Ručevskis, S. and Kaewunruen, S. (2019), "Mode shape curvature squares method for crack detection in railway prestressed concrete sleepers", *Eng. Fail. Anal.*, **105**, 386-401. https://doi.org/https://doi.org/10.1016/j.engfailanal.2019.07.020
Jayasundara, N., Thambiratnam, D.P., Chan, T.H.T. and Nguyen, A. (2020), "Damage detection and quantification in deck type arch bridges using vibration based methods and artificial neural networks", *Eng. Fail. Anal.*, **109**, 19. https://doi.org/10.1016/j.engfailanal.2019.104265
Li, J., Dackermann, U., Xu, Y.-L. and Samali, B. (2011), "Damage identification in civil engineering structures utilizing pca-compressed residual frequency response functions and neural network ensembles", *Struct. Control Health Monit.*, **18**(2), 207-226. https://doi.org/10.1002/stc.369
Lim, H.C., Ong, Z.C., Ismail, Z. and Khoo, S.Y. (2019), "A performance study of controlled impact timing on harmonics reduction in operational modal testing", *J. Dyn. Syst. Measur. Control-Transact. ASME*, **141**(3). https://doi.org/10.1115/1.4041609
Liu, C., Nagler, O., Tremmel, F., Unterreitmeier, M., Frick, J.J., Patil, R.P., Gu, X.W. and Senesky, D.G. (2022), "Cluster-based acoustic emission signal processing and loading rate effects study of nanoindentation on thin film stack structures", *MSSP*, **165**, 18. https://doi.org/10.1016/j.ymssp.2021.108301
Mekjavic, I. and Damjanovic, D. (2017), "Damage assessment in bridges based on measured natural frequencies", *Int. J. Struct. Stab. Dyn.*, **17**(2). https://doi.org/10.1142/s0219455417500225
Mousavi, A.A., Zhang, C.W., Masri, S.F. and Gholipour, G. (2021), "Damage detection and localization of a steel truss bridge model subjected to impact and white noise excitations using empirical wavelet transform neural network approach", *Measurement*, **185**, 19. https://doi.org/10.1016/j.measurement.2021.110060
Nguyen, D.H., Tran-Ngoc, H., Bui-Tien, T., De Roeck, G. and Wahab, M.A. (2020), "Damage detection in truss bridges using transmissibility and machine learning algorithm: Application to nam o bridge", *Smart Struct. Syst., Int. J.*, **26**(1), 35-47. https://doi.org/10.12989/sss.2020.26.1.035
Nick, H., Aziminejad, A., Hosseini, M.H. and Laknejadi, K. (2021), "Damage identification in steel girder bridges using modal strain energy-based damage index method and artificial neural network", *Eng. Fail. Anal.*, **119**, 20. https://doi.org/10.1016/j.engfailanal.2020.105010
Ong, Z.C., Lim, H.C., Brandt, A., Ismail, Z. and Khoo, S.Y. (2019), "An inconsistent phase selection assessment for harmonic peaks elimination in operational modal testing", *Arch. Appl. Mech.*, **89**(12), 2415-2430. https://doi.org/10.1007/s00419-019-01584-3
Padil, K.H., Bakhary, N., Abdulkareem, M., Li, J. and Hao, H. (2020), "Non-probabilistic method to consider uncertainties in frequency response function for vibration-based damage detection using artificial neural network", *J. Sound Vib.*, **467**, 115069. https://doi.org/https://doi.org/10.1016/j.jsv.2019.115069
Porcu, M.C., Patteri, D.M., Melis, S. and Aymerich, F. (2019), "Effectiveness of the frf curvature technique for structural health monitoring", *Constr. Build. Mater.*, **226**, 173-187. https://doi.org/https://doi.org/10.1016/j.conbuildmat.2019.07.123
Sarmadi, H., Entezami, A., Salar, M. and De Michele, C. (2021), "Bridge health monitoring in environmental variability by new clustering and threshold estimation methods", *J. Civil Struct. Health Monitor.*, **11**(3), 629-644. https://doi.org/10.1007/s13349-021-00472-1
Sha, G., Radzieński, M., Cao, M. and Ostachowicz, W. (2019), "A novel method for single and multiple damage detection in beams using relative natural frequency changes", *MSSP*, **132**, 335-352. https://doi.org/https://doi.org/10.1016/j.ymssp.2019.06.027
Siow, P.Y., Ong, Z.C., Khoo, S.Y. and Lim, K.S. (2021), "Damage sensitive pca-frf feature in unsupervised machine learning for damage detection of plate-like structures", *Int. J. Struct. Stab. Dyn.*, **21**(2), 29. https://doi.org/10.1142/s0219455421500280
Solimine, J., Niezrecki, C. and Inalpolat, M. (2020), "An experimental investigation into passive acoustic damage detection for structural health monitoring of wind turbine blades", *Struct. Health Monitor.*, **19**(6), 1711-1725. https://doi.org/10.1177/1475921719895588
Tran, C.J., Mora, O.E., Fayne, J.V. and Lenzano, M.G. (2019), "Unsupervised classification for landslide detection from airborne laser scanning", *Geosciences*, **9**(5), p. 221. https://doi.org/10.3390/geosciences9050221
Vafaei, M. and Alih, S.C. (2018), "Adequacy of first mode shape differences for damage identification of cantilever structures using neural networks", *Neural Comput. Applicat.*, **30**(8), 2509-2518. https://doi.org/10.1007/s00521-017-2846-6
Wang, S. and Xu, M. (2019), "Modal strain energy-based structural damage identification: A review and comparative study", *Struct. Eng. Int.*, **29**(2), 234-248. https://doi.org/10.1080/10168664.2018.1507607
Wickramasinghe, W.R., Thambiratnam, D.P. and Chan, T.H.T. (2020), "Damage detection in a suspension bridge using modal flexibility method", *Eng. Fail. Anal.*, **107**, p. 104194. https://doi.org/10.1016/j.engfailanal.2019.104194
Xu, Y.L., Huang, Q., Zhan, S., Su, Z.Q. and Liu, H.J. (2014), "Frf-based structural damage detection of controlled buildings with podium structures: Experimental investigation", *J. Sound Vib.*, **333**(13), 2762-2775. https://doi.org/10.1016/j.jsv.2014.02.010
Xu, W., Zhu, W.D., Xu, Y.F. and Cao, M.S. (2020), "A comparative study on structural damage detection using derivatives of laser-measured flexural and longitudinal vibration shapes", *J. Nondestr. Eval.*, **39**(3), 17. https://doi.org/10.1007/s10921-020-00702-4
Zhu, X., Wang, Y., Li, Y., Tan, Y., Wang, G. and Song, Q. (2019), "A new unsupervised feature selection algorithm using similarity-based feature clustering", *Computat. Intell.*, **35**(1), 2-22. https://doi.org/10.1111/coin.12192

HJ